RESEARCH ARTICLE   OPEN ACCESS

Automated Decision Support System for Pathology of Diabetic Retinopathy from OCT

Catherine Todd[1], Paola Salvetti[2], Katy Naylor[2], Chisom Nnorom[3]

1 (Department of Computer Science and Engineering, Hawaii Pacific University, Hawaii
Email: cghourani@hpu.edu)
2 (Opthalmology, Moorfields Eye Hospital Dubai, United Arab Emirates
Email: paola.salvetti@moorfields.ae, katy.naylor@moorfields.ae)
3 (Department of Engineering and Information Sciences, University of Wollongong in Dubai, United Arab Emirates
Email: cun998@uowdubai.ac.ae)

Abstract:

Diabetic retinopathy is a complication of diabetes causing progressive damage to the retina, located at the back of the eye, potentially leading to clouded vision or blindness. Disease signs may be visualized by Optical Coherence Tomography (OCT) and include formation of new and weaker blood vessels, fluid accumulation, exudates and changes to Retinal Vascular Geometry (RVG). Presence of these indicators can provide information as to the stage of the disease. Image-processing strategies are applied for the automated detection, segmentation, extraction, classification toward likelihood estimation of progression of diabetic retinopathy to visual biomarkers present in OCT, using time-sequenced data in the early stages of the disease. Gabor and Savitsky-Golay filtering enables extraction of the vessel map and fuzzy control for segmentation of hard exudates. Feature data are extracted using bounding boxes, vector map and connected component methodology for binary decision tree classifier construction, training and testing. Feature values comprising classifier nodes include: exudate features of compactness, area, convexity and form factor, in addition to vessel features: width, elongation, bifurcation angles, form factor and solidity. Classifier accuracy is 93.3%, with 6.7% misclassification and 0% false-negative classification. Automated image processing of diabetic retinopathy is achieved with high classification accuracy for the extraction of vessel map and hard exudate biomarkers from OCT. Application of smoothing algorithms and removal of vessel map shadows may further improve classification accuracy.

Keywords ——**Retinopathy, Medical Image Processing, Pathological Progression, Vessel Map Segmentation, Hard Exudate Extraction, Image Classification**

I. INTRODUCTION

Diabetic retinopathy is a complication of diabetes causing progressive damage to the retina, located at the back of the eye, potentially leading to clouded vision or blindness. The retinopathy may be classified as non-proliferative or proliferative; the former subdivided into three sub-stages of mild, moderate and severe Non-Proliferative Retinopathy (NPDR). Disease symptoms include formation of new, weaker blood vessels (neovascularization), fluid accumulation, presence of exudates and Retinal Vascular Geometry (RVG) changes [1]. Presence, extent and morphology of these indicators can provide information as to the stage of the disease [1].

During the first stage of NPDR patients may exhibit no signs of clinically significant retinopathy. However, at this stage microaneurysms may start to form and fluid leakage into the retina may begin [1]. The risk of vision loss in mild NPDR is low, however a high microaneurysm count can be an indicator of disease progression [1], [2], [3]. In moderate NPDR other signs may include soft exudates and microvascular abnormalities [1]. Hard exudates may translate into areas of retinal thickening [1]. Approximately 50% of patients with moderate NPDR progress to Proliferative Diabetic Retinopathy (PDR) [1].

PDR represents an advanced form of the disease where circulation problems may lead to the retina being deprived of oxygen. Patients at this stage also experience a growth in neovascularization and possible vascular tearing with leakage of blood into the retina and vitreous, resulting in clouded vision

[1]. Patients in the stage of PDR have high risk of suffering vision loss within two years if the disease goes untreated [1]. PDR may lead to other complications such as retinal detachment or glaucoma.

Chemical biomarkers in the vitreous are identified as part of diabetic retinopathy. Changes in the production of proteins such as Hepathocyte Growth Factor (HGF), Vascular Endothelial Growth Factor (VEGF) and Nitric Oxide (NO) can lead to changes in retinal blood vessel function [4]. This in turn changes RVG parameters which can be visualized and detected using imaging modalities such as Optical Coherence Tomography (OCT) [4], although RVG changes may be subtle and difficult to detect, especially in the early stages of the disease. Regular patient scanning can help with early detection and identification of disease progression [2].

This paper proposes automated image-processing strategies for detection, segmentation, extraction, and classification toward likelihood of progression of diabetic retinopathy. Visual biomarkers present in OCT are used toward improved classification accuracy and estimation of disease progression, using time-sequenced data specifically in the early stages of the disease (NPDR from mild to moderate). Methods and results from this study may be useful in determining the feature set for diagnosis of early stage disease as well as likelihood of progression and further, to help reduce number of patient visits and costs associated with medical consultations.

II. BACKGROUND

This research applies image-based methods for the detection of features corresponding to the presence of diabetic retinopathy. This criterion limits the feature set of interest as certain indicators and biomarkers of diabetic retinopathy cannot be detected through non-invasive imaging techniques. In the research literature, image-based features extracted for subsequent identification, segmentation, extraction and classification toward determination of diabetic retinopathy comprise RVG parameters including changes in vessel width, bifurcation angles, neovascularization, hard exudates and microaneurysms. These may be

combined with other patient-specific information, such as age and presence of hypertension, to determine the presence of retinopathy and toward likelihood estimation of disease progression.

A. Visual Biomarkers in OCT

Biomarkers are characteristics that provide facilitation of status indication as normal, pathological or pharmacological response to treatment in biological processes [3]. These features can be extracted through imaging, chemical testing or visual inspection [3]. Chemical biomarkers such as measures of different protein levels in the retinal blood vessels and vitreous provide similar indication but are not evident in medical scan data [5]. These include Vascular Endothelial Growth Factor (VEGF), Interleukin-6 (IL-6), Erythropoietin (EPO), NO, Platelet-Derived Growth Factor BB chain (PDGF-BB), HGF and Transforming Growth Factor Beta (TGF-β) [5], [6]. Retinal vessels tend to exhibit damage as a result of complications associated with diabetes [3] and are identifiable and measurable through retinal image-based examination [2], [3]. These retinal vessel changes may indicate pathology and progression for NPDR and PDR candidates.

Morphological changes in vessel structure including width, bifurcation angle and microaneurysms [1], [4], [7], [8], [9] in addition to the formation of newer, weaker vessels (neovascularisation) [1] are features that are identifiable within retinal scans that have proven useful for determination of pathology status in diabetics [1], [4], [7], [8], [9]. These features may be extracted from primary biomarkers as well as secondary changes such as formation of hard exudates [2], [4], [6], [10] [11]. Advances in non-invasive retinal imaging methods have made possible the accurate imaging and measurement of widths and angles of vascular features [3], [12], in addition to their correlation with a status of pathology [13].

A relationship between the retinal vascular caliber and incidence as well as progression of diabetic retinopathy has been established [13] in type 1 diabetics [13], as well as a correlation between increased retinopathy severity and increased widths of vascular segments, both in

arteries and veins [2], [3]. Increase in total bifurcation angles of parent and child vessel are also associated with an increase in the severity of diabetic retinopathy [2].

Microaneurysms are evident from notable localized bulging of retinal blood vessels [8], [13]. Statistical studies reveal that expansions resulting from microaneurysms cause a disturbance in the normal flow pattern leading to change in the force and pressure along the vessel [13], with such signs detectable through fundus imaging [8]. A two-step or greater increase in microaneurysm count in accordance with the Early Treatment Diabetic Retinopathy Study (ETDRS) scale is indicative of disease progression in type 1 and type 2 diabetics [8]. The relationship between the scores of microaneurysms and ETDRS retinopathy level showed direct proportionality at the end of the 4.6 year study [8].

Hard exudates occur as a result of leakage of proteins and lipids from the blood vessels in the retina. These appear as bright yellow spots in color fundus images and bright white spots in grey-scale images [2], [6], [11]. Hard exudates serve as indicators of the presence of diabetic retinopathy; qualified therefore as a secondary sign rather than a biomarker [14]. In addition to hard exudates, microaneurysms and intra-retinal vascular abnormalities, signs of the disease also include haemorrhages, cotton wool spots and macular oedema [10]. It is important to recognize that signs of diabetic retinopathy may also be shared with other diseases, therefore complicating the process of classification and likelihood estimation of image-based pathology for solely diabetic retinopathy.

B. Detection and Segmentation of Vessel Maps and Hard Exudates

A variety of methods have been applied for pre-processing and detection of features within the eye of candidates with retinopathy. Median filtering and histogram equalization are applied by Torok et al. [15] for contrast enhancement and image smoothening. Texture analysis is applied for image enhancement [11] including the match filtering on green channel [11], [15] and histogram grey level analysis [11]. For detection of exudates and the vessel map, Sobel and Canny edge detectors have

been applied [14]. The optic disc is removed from the image and then the Spatially Weighted Fuzzy C-Means (SWFCM) algorithm is applied for the segmentation of hard exudates [11], in addition to median filtering, matched filtering and Gaussian Point Spread Function (PSF) [4], [11], [14]. The Matched filter is a Gaussian filter that has previously been applied to retinal images for the extraction of retinal vessels [11], [16], [17], [18], [19], with the Matched Filter-First Derivative of Gaussian (MF-FDoG) approach applied to differentiate between vessel and non-vessel segments [11], [16], [18], [19], and accurately extract vessels of various widths to create an isolated vessel map [16].

C. Feature Set Extraction and Pathology

Morphological operations have been applied on retinal scans for extraction of features of the vessel map, including measures of segmented component compactness, form factor, extent, elongation factor and solidity [16]. Form factor and compactness revealed success for classification of vessel or non-vessel components, with compactness providing greatest feature accuracy [16]. Support Vector Machine (SVM) and a Radial Basis Function (RBF) kernel provided utility for classification of the extracted feature vector set as either vessel or non-vessel [16]. Classification is intended to aid clinical analysis of vessel and non-vessel maps of individual patients generated in a sequential time-lapse for establishing progression of diabetic retinopathy [16].

Application of bounding boxes has proved useful for extraction of vascular width information and bifurcation angles [2]. Vessel widths and spread across retinal image were determined by placing bounding rectangles over the centerlines of each vascular segment [2]. For every nominated vessel, the measured parameters included absolute width measurements of parent vessel, larger branch and smaller branch, overall bifurcation angle, and the branching angle between the larger vessel and smaller vessel [2]. Bifurcation angles were successfully obtained using this approach, however the process was manual.

Top hat transforms enable extraction of small features within an image. The top hat transform

applies morphological reconstruction [15] after which the reconstructed image is opened by a 10 by 10 disk shape for the detection of small circular objects within the scan, the result of this procedure being a group of possible microaneurysm candidates [15]. Properties of these candidates are calculated: area, rotational inertia, mean intensity both in the green plane and the opened image and the standard deviation of pixel intensity in the green plane [15].

Statistical methods including multiple linear regression [2], Fisher-protected Least Significant Difference (FLSD) and one-way ANOVA have been applied to analyze the effects of demographic factors combined with RVG parameters on the occurrence and progression of diabetic retinopathy amongst age-matched study subjects [2]. The analysis revealed progressive increase in values of vascular properties with the progression of retinopathy [2]. Mean values of RVG features were used for the classification of retinopathy grade in addition to other clinical and demographic information [2]. One-way ANOVA was used in the assessment of intra-observer repeatability and average variation coefficients were found as 4.2% for vascular width measurements and 3.8% for angular measurements [2]. RVG parameters vary with distance from the Optic Nerve Hypoplasia (ONH); the patient with the lowest mean distance from ONH was chosen as a reference [2]. Bifurcation angles for the other patients were progressively eliminated, starting with the most distant until the mean distance ratio was close to that of the reference candidate [2]. Analysis was done including branching angle parameters as well as vessel width parameters [2]. A 97.6% sensitivity and 90% specificity were achieved for classification accuracy with results showing that the deflection angles had minimal effect on the grading of the retinopathy [2].

Gradient Boosting Machine is implemented for the classification of microaneurysm candidates [15]. Classifier testing accuracy is obtained by comparison with manually marked microaneurysms and is further trained using a Naïve Bayes Classifier, its performance assessed with the use of a 10-fold cross-validation method [15]. Fundus images were processed with a microaneurysm detection algorithm, a threshold value is then computed for classification as either microaneurysm or non-microaneurysm, with a microaneurysm count calculated and used for the purposes of pathology [15]. Results produced 84% sensitivity and 81% specificity [15].

D. Likelihood Estimation for Pathological Progression

Existing studies [13] have suggested a correlation between changes in RVG parameters, count of microaneurysms and progression of diabetic retinopathy. Other clinical risk factors including high cholesterol and high blood pressure could further increase the risk of progression to proliferative diabetic retinopathy [13]. Of interest to this study is the identification, quantification and appropriate structure (combination) of a set of features that will accurately detect, classify and predict the likelihood of progression of diabetic retinopathy in a candidate, through the application of novel image processing strategies. This is the focus of future research work, in addition to removing vessel shadows in the segmentation stage.

III.   METHOD

A. Data Acquisition; OCT Retinal Scans

In this research, grey-scale images comprised time-sequenced Optical Coherence Tomography (OCT) scans taken during series of follow-up patient visits by an experienced retinal surgeon using the Heidelberg Engineering Spectralis HRA+OCT (S3600-IFP). The OCT machine co-registered images within the volume scan and between patient scans using offset, dual laser technologies, ensuring alignment of anatomical structures. This inbuilt, automatic image-alignment technology overcomes co-registration shortcomings previously a concern among research studies [20], [21] that applied algorithms including SURF [20] and SIFT [21] for image co-registration and orientation alignment post-image capture. Retinal scans were acquired at an acquisition angle of 30° and at varying densities; providing variation in distance between consecutive images within a particular set of scans. Inter-image distance sampling was performed in an effort to determine the minimum density of acquisition to avoid loss of feature-based information. Scans were grouped

according to time of capture, density at which the images were taken and eye (left or right) under processing. Images were imported into MATLAB for pre-processing and structure isolation (refer Fig. 1.). Images within a group were automatically cropped into transverse and axial views of the retina, and then loaded into a volume-based cell for processing.
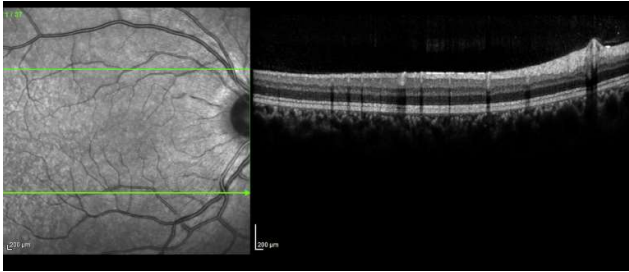

Fig. 1 An Example of an Original Retinal Image Captured with OCT

B. Vessel Map Isolation; Edge Detection and Filter Methods

A variety of methods were applied for automated detection and segmentation of the vessel map from non-vessel data. Techniques included: Sobel and Canny edge detectors, Matched, Gaussian and Gabor Filters. Success criteria included successful, lossless extraction of the vessel map with the exclusion of surrounding structures.

1) *Edge Detection:* Results of Sobel and Canny edge detectors included non-vessel data; quantitative and qualitative evaluation of image results revealed vessel shadows and retinal vessels evident in the transverse view of the retina. Figs. 2., 3. and 4. show the original axial OCT image, the output of the Canny filter and the output of the Sobel filter respectively. Elimination of vessel shadows in transverse images of the retina has previously been achieved using Statistical Shape Models (SSMs) and Principal Component Analysis (PCA) to represent an average model of vessels within the scan [10]. In addition to SSMs, a shadow graph may be applied to the retinal scan for pixel threshold cut-off, based on the vertical intensity distribution of pixels [10]. Within this process a pixel centred in the image is selected as the cut-off point if intensities are evenly distributed [10]. The cut-off point moves upward in the scan if a sharp decrease in intensity values is identified [10].

2) *Gaussian Filtering and Adaptive Thresholding:*

For more accurate extraction of the vessel map from non-vessel data, a histogram equalized version of the retinal scan is subjected to a First Derivative of Gaussian (FDoG) Filter followed by adaptive thresholding. Local thresholding enables vessel pixel grouping. Connected-component thresholding is applied to produce the final vessel map.

The FDoG filter is designed as in [16] and implemented. The filter creates two Gaussian kernels with σ = 0.5 for the x and y directions with the kernel for the y-axis being a transpose of that created for the x-axis. The kernels are created and then convolved with the histogram equalized image after which the magnitude of the filter response to both kernels is calculated and displayed as the resultant image. A mean filter is then applied for the local thresholding process using a 13*13 sized window. Connected-component thresholding is finally applied to the result for elimination of image noise and to produce the final vessel map. Sample results are captured in Figs. 5. through 9., derived from the original, cropped axial image shown previously in Fig. 2.

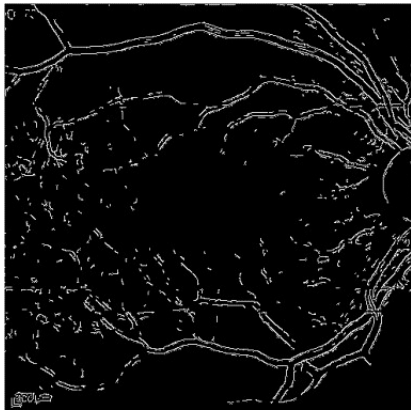Fig. 2 Original, Cropped OCT Image: Axial View

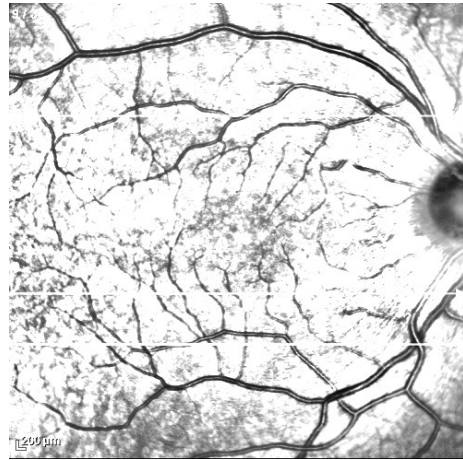Fig. 3 Example of Canny Edge Detector Resultant Image
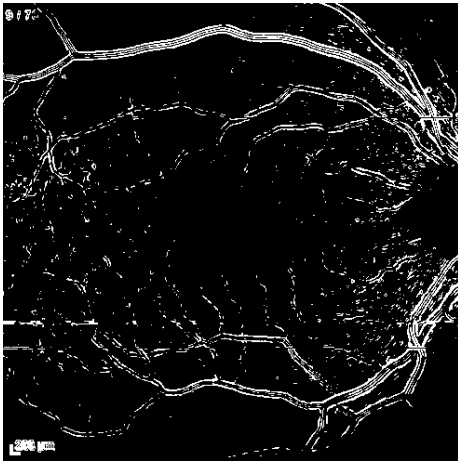

Fig. 6 The Gaussian-Gradient Image

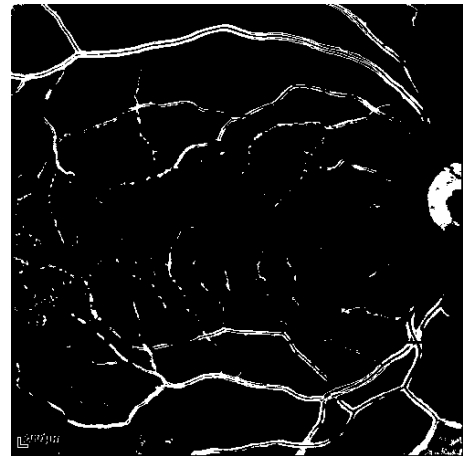Fig. 4 Example of Sobel Edge Detector Resultant Image

Fig. 7 Result of Global Thresholding on the Gaussian Image
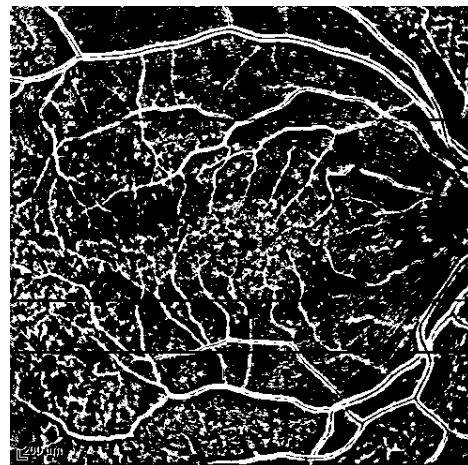

Fig. 5 The Histogram Equalized Image

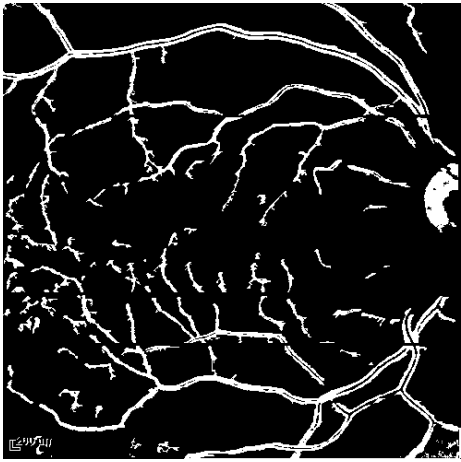Fig. 8 Result of Mean Filtering on the Histogram Equalized Image

Fig. 9 Final Vessel Image as Derived by Application of Connected-Component Analysis on Data Produced and Shown in Fig. 7 and Fig. 8.

similar methods applied to the fundus images (Figs. 11 and 12); where the MF-FDoG were tested on fundus images from the DRIVE database [22] directly and results showed notable removal of background information.
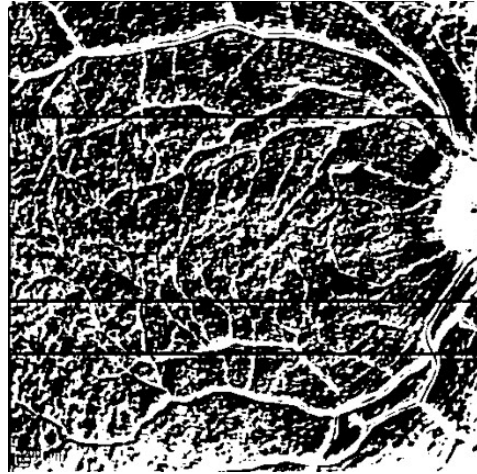

Fig. 10 MF-DoG Applied to the OCT Axial Image

3) *Matched Filtering*:

The vessel map is separately isolated using a Matched Filter (MF) that utilizes a Gaussian function and a minimization factor which normalizes the mean of the filter to zero-smooth the image background. The Gaussian function defining the filter creates mask kernels for both the x and y directions; the y-gradient mask is the transpose of the x-gradient mask. MF kernel parameters are varied with a standard deviation from 1 to 1.5, and filter length 5 to 9. These masks are applied to the histogram equalized version of the image giving a response that is the Gaussian image. A mean filter of w*w dimensions that has all filter elements set to $1/w^2$, with w set to 31, is then applied to the Gaussian image. The resultant image then normalized with pixel values from 0 to 1. This normalized image is used for threshold value calculation. The final image from this process is obtained by performing a logical OR operation of the threshold values and the MF.

Results were compared with vessel maps in the literature, in work that applied MFs to retinal images captured with a fundus camera [11], [16], [17], [18], [19]. Image results of the developed MF-FDoG filter applied to retinal scans acquired through OCT revealed more inclusion of background information resulting from higher texture detail obtained (Fig. 10) as compared with
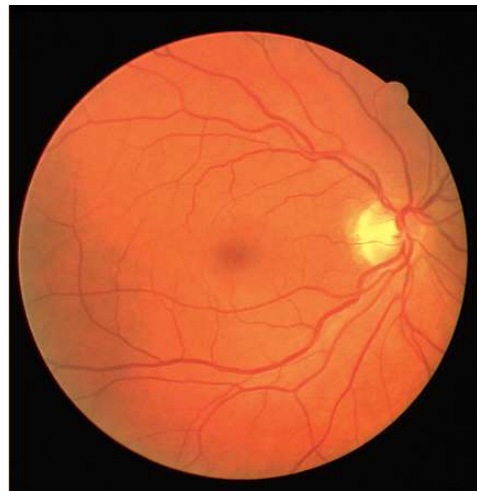

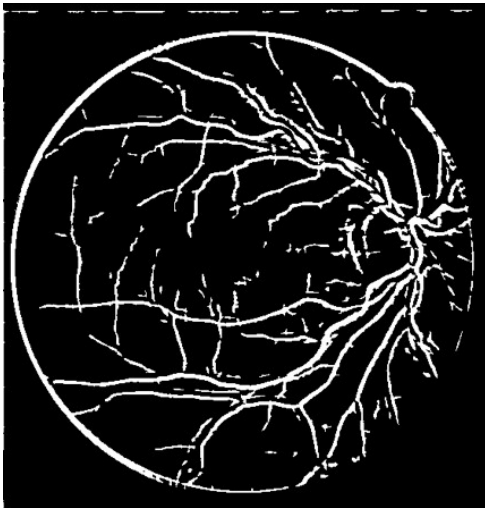Fig. 11 Original Fundus Image of the Retina, from the DRIVE Database

Fig. 12 MF-DoG Applied to the Data from the Image shown in Fig. 12

Retinal images captured from OCT contain higher bit-depth and spatial resolution than Fundus images. While automatic isolation of the vessel map from surrounding detail proves challenging in this context, shape-based properties of vessel behaviour may enable more accurate segmentation. It is noted in axial OCT images that retinal vessels tend to assume a centripetal formation towards the fovea. Isolation of the vessel map with filters that consider vessel orientation were deemed to offer utility in this regard.

4) *Gabor and Savitsky-Golay Filtering*:

Gabor filtering implements a Gaussian filter that considers image pixel orientation [23] [24]. A Gabor filter has been implemented based on the existing methods [23], [24] for vessel map segmentation. A kernel size 15*15 is created with filter versions implemented for the detection of vessels at different orientations by rotating the initial filter kernel between 0º and 180º in increments of 1º. After application of all versions of the rotated kernels, the maximum response of each pixel is retained and logarithmic normalization is then applied to the image to obtain total filter response. Thresholding is then applied for removal of background information, providing the isolated vessel map. Adaptive histogram equalization was applied to the output image from the Gabor filter to increase contrast between the vessel map and image background. The Savitsky-Golay filter was then applied for estimation and removal of background

pixels. The Savitsky-Golay filter is a smoothing filter based on a local least-squares polynomial approximation. After Savitsky-Golay filtering, small regions are detected and removed from the image to obtain the final, isolated vessel map (Fig. 13).
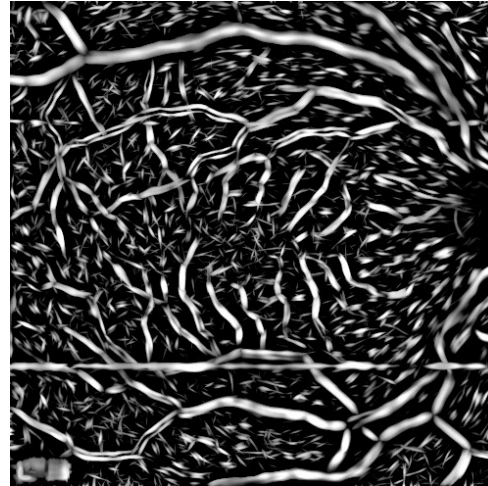

Fig. 13 Final Vessel Map Image Following Gabor and Savitsky-Golay Filtering

C. Delineation and Quantification of Hard Exudates

A Fuzzy C-means (FCM) algorithm is applied for the clustering and detection of pixels representing exudates first in the axial OCT scan, and then in the transverse OCT scan. The algorithm operates as follows: first, pixel degree of membership is initialized to a normalized value within the range [0, 1]. Centre vectors are then calculated using techniques defined in [14]; the result of which is used for updating the degree of membership of all pixels. The present value of the membership function is subtracted from the previous value: a process which is repeated until the termination criterion is reached, wherein final clusters are displayed, returning an image of the detected exudate pixels.

Review of results revealed existence of an artefact: a bright, round spot in centre of the axial image slice as a result of light reflection from the lens, with dependency on the distribution of crystalline fibres in the lens of the patient under examination. This anomaly was not evident in all images, yet analysis of only the transverse plane proved more reliable in accuracy of exudate

detection. The cropped image containing only the transverse view is input to the FCM algorithm for detection of exudate clusters, modified to segment the contents of the image into five distinct clusters. The cluster centres and proximal areas are compared; the largest clusters are retained. An original, cropped transverse image (Fig. 14) and final sample result (Fig. 15) are shown.
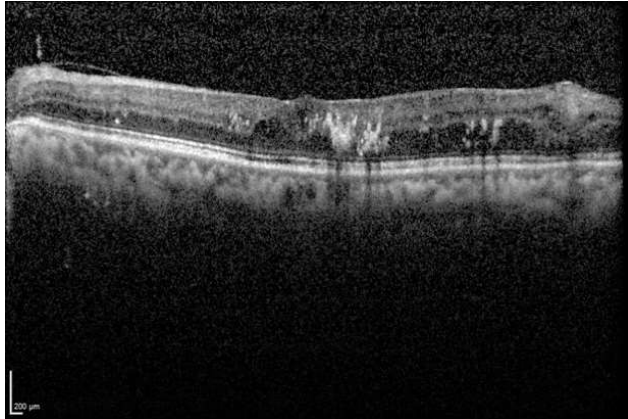

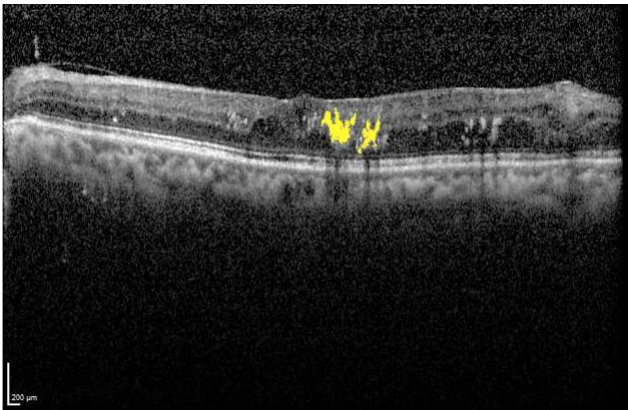Fig. 14 Original, Cropped Transverse OCT Image of the Retina

Fig. 15 Result of the FCM Algorithm with Exudate Extraction shown as Yellow Region; this is Superimposed onto the Original Transverse OCT Image Data as in Fig. 14

Morphological features are then computed from exudate clusters, including: eccentricity, area and equivalent diameter. Due to retention criteria associated with larger exudate clusters, smaller exudates may be misclassified as false-negatives. This retention/exclusion criteria should be further examined to reduce the false-negative misclassification rate due to smaller yet suspicious regions.

D. Quantification of Biomarkers: Feature Extraction

To provide quantitative comparison of vascular segment features for pathology diagnosis, microaneurysms and RVG parameters are extracted from the vessel map obtained from the final image result following Gabor and Savitsky-Golay filtering. Morphology of exudates are also computed for use in classification. The top hat transform [15] is applied for detection and quantification of microaneurysms. For computation of RVG parameters, including vessel width and bifurcation angles, bounding rectangles are utilized. For extraction of parameters from the isolated vessel map, image results obtained following the Gabor and Savitsky-Golay filtering process were first binarized. Background information was reduced by eliminating regions whose features did not satisfy criteria relating to perimeter and area.

Image results from FCM methods were used for computation of morphological features including eccentricity, area and equivalent diameter for retention and feature calculation of exudate clusters. Final clusters which satisfied parameter criterion for inclusion were superimposed onto the original image to obtain the outline and exudate location.

Exudate extent, solidity, elongation, compactness and form factor were computed. Thresholding was applied to determine feature values best representative of biomarker indication. Exudate diameter and perimeter were computed yet considerable variation in these values rendered these features inadequate as pathology indicators.

Feature parameters are computed for 520 images. Statistical variance of feature parameters are summarized in Table I, including minimum and maximum value, average value and standard deviation for all 520 test data samples. Program performance took 15 seconds per image on average (one batch of 49 images took 780 seconds) to attain quantified features following digitized OCT image input to MATLAB. All aspects of the program after image input were automated.

TABLE I
FEATURE SET RESULTS FOR 520 IMAGES WITH STATISTICAL VARIATION

Biomarker of Relevance	Feature	Mean	Min., Max.	Std. Dev.
Vessel Classify	Area	451.4547	1, 5258	622.773

Vessel Classify	Bounding box of Vessel Regions (width, height)	(26.9201, 59.3433)	(1, 1), (156, 495)	(21.606, 67.2315)
Vessel Dilation	Width	6.6267	1, 16.6667	2.4915
Exudate Presence	Extent of Exudates	0.5218	0.2047, 0.8815	0.0942
Exudate Presence	Solidity	0.7670	0.4192, 0.9610	0.0870
Exudate Presence	Elongation	0.4820	0.0389, 0.7619	0.3165
Exudate Presence	Compactness	1	1, 1	0
Exudate Presence	Form Factor	0.6365	0.1131, 0.8999	0.1577

E. Diabetic Pathology and Classification

Following feature set extraction and quantification, the classifier output provides a final diagnosis of presence or non-presence of diabetic retinopathy. Biomarkers representing exudate presence and morphology, vessel map abnormalities (microaneurysms) and changes to vessel properties (vessel width, bifurcation angle) indicate the presence of diabetic retinopathy; the classifier is constructed with these criteria established.

Initial classifier design produced high misclassification rates based on the presence of exudates. Misclassification results were then reduced by setting thresholds for those features that considered circularity of exudate regions. Classification based on exudate information included eccentricity, form factor and ratio of width to length of the corresponding bounding box containing the region of interest. Threshold values for associated exudate features were set through experimentation to reduce false-positive rates.

SVMs have shown success in the isolation of vessel maps for classification of features as vessel or non-vessel components [16]. In this work, quantified feature data as extracted using bounding boxes, vector map and connected component methodology, unique to this work, are applied to construct, train and test a binary decision tree classifier. Quantified feature set information were used for classifier construction and testing,

including exudate compactness, area, convexity and form factor, in addition to vessel width, elongation, bifurcation angles, form factor and solidity. Values representing the difference between vessel widths and exudate count in time-sequenced images (between patient visits) were input to the decision tree classifier. The classifier was trained using information obtained from 32 images after which its performance was tested on 84 independent images: a summary of results is provided in Table II.

TABLE III
SUMMARY OF CLASSIFICATION RESULTS FOR 84 IMAGES FROM 15 IMAGE VOLUMES

Image Volume Set (Identifier)	Width Difference	Exudate Number	Classifier Results	False Positive/ Negative
Case1,V1, LED1	0	1	'Pa'	-
Case1,V1, REstd.	0	0	'H'	-
Case3,V1, REstd.	0	5	'Pa'	-
Case1,V3, LEstd.	0.3	0	'H'	-
Case2,V1, LE std.	0	3	'Pa'	-
Case1,V2, LED3	0	0	'H'	-
Case1,V2, LED1	0	0	'H'	-
Case1,V1, RED1	0	0	'H'	-
Case1,V3, RED4	0.3	0	'H'	-
Case1,V1, LED4	0	0	'H'	-
Case1,V2, LED2	0	0	'H'	-
Case2,V1, REstd.	0	5	'Pa'	-
Case1,V1, LED2	0	2	'Pa'	False Positive
Case1,V1, RED2	0	0	'H'	-
Case1,V4, LED5	0	0	'H'	-

The classifier is designed to group the images into three distinct groups, with output: 'Pa' representing those images classified as pathological, 'Pr' denoting images that show signs of progression

of diabetic retinopathy and 'H' for images of healthy eyes (non-pathological). During testing, bifurcation angles did not vary enough between image output types and as such, this feature was excluded from the final decision tree since it was not a useful classification feature. A graph depicting the final decision tree is displayed in Fig. 16, where variable *exuCount* represents the number of exudates present as determined by extracted and quantified exudate compactness, area, convexity and form factor. Variable *widthDiff*, is computed with values representing vessel width, elongation, bifurcation angles, form factor and solidity. Values representing the difference between vessel morphology and exudate count in time-sequenced images (between patient visits) were input to the decision tree classifier. Classifier accuracy achieved is 93.3%, with 6.7% misclassification and 0% false-negative classification.
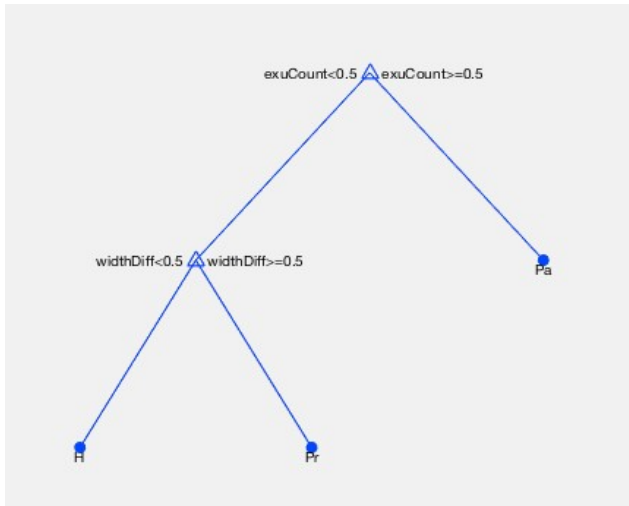

Fig. 16 Decision Tree Classifier with Parameter Settings

IV. DISCUSSION

Features representative of diabetic retinopathy biomarkers in OCT retinal images were extracted and quantified in addition to the application of automated image processing strategies, including edge detection, filtering methods, top hat transformations and fuzzy control techniques for isolation of the vessel map, hard exudates and microaneurysms. In the literature, techniques applied were focused on extraction of features from color Fundus images, with few diagnostic studies applying image-based techniques to OCT images.

Automated segmentation of the vessel map proved challenging: a variety of techniques including edge detection and filtering were applied yet isolation of the map from surrounding non-vessel is a difficult process given the extent of detail contained in retinal OCT images. Gabor and Savitsky-Golay filter combination provided the best results in this respect as compared to Matched filtering.

Exudate detection and segmentation was performed using fuzzy clustering and morphological features were considered for elimination of non-exudate regions. Initially, these processes combined with feature quantification into a binary decision tree classifier produced high misclassification results for both false positive and false negative classifications with false-positive results primarily due to the extent of image detail and false-negatives largely due to background image noise. Threshold-based approaches and properties of circularity for identified regions reduced misclassification rates to 6.7% (false-positive rate) with 0% false-negative rate and an overall classification accuracy of 93.3%. In comparison to the literature [15] and [2], with 81% and 90% specificity respectively, and 84% and 97.6% sensitivity respectively, this classification result is credible. However, it is suggested that misclassification rates for exudates could be further reduced through the application of smoothing filters for noise removal and contrast adjustment to avoid detection of retinal boundaries as exudate clusters.

V. CONCLUSION AND RECOMMENDATION

This study was conducted to improve early detection of biomarkers indicting diabetic retinopathy through the design of an automated, computerized decision support system. Automated image processing of diabetic retinopathy has been achieved with high classification accuracy (93.3%) for the extraction of vessel map and hard exudate biomarkers from OCT. A main advantage of using OCT images as opposed to fundus color images is that the wavelength used to generate the images (810 nm) has higher penetration and is less absorbed but the ocular structures than the white

light used to generate the color fundus images. This combined with the confocality of the Spectralis instruments provides with images that have less confounding factors and here hence more suitable to be used with an automated feature detection tool. Application of smoothing algorithms and removal of vessel map shadows may improve classification accuracy.

The advantages of this automated system are largely reduced when applied to patient datasets that display advanced stages of retinopathy particularly due to observable and significant damage to the retina. Early intervention is key to treating and maintaining the disease. The importance of obtaining an accurate, isolated vessel map in a study such as this should not be underestimated. Several features may be extracted from the vessel map that can be successfully used for final diagnosis. Accuracy in vessel map extraction is necessary for more accurate vessel boundary detection, vessel width and bifurcation angle detections, that will help reduce misclassification results. Further pre-processing techniques may assist in this regard, for elimination of background information. Improvements in detailed computation of vessel width may further improve classification results, with suggestion for extraction from the transverse image plane with application of techniques for removal of vessel shadows. Future research work is focused on addressing these research challenges in addition to using the feature data and classification results to automatically determine likelihood estimation of pathological progression of diabetic retinopathy, using time-sequence image volumes acquired with OCT.

REFERENCES

1. *Y. Priestley, M. Hoepf, et al., Comprehensive Review of the Effects of Diabetes on Ocular Health, Expert Rev. Ophthalmol., 2010, vol. 5, no. 4, pp. 557–577.*

2. *M. S. Habib, B. Al-Diri, A. Hunter, et al., The Association between Retinal Vascular Geometry Changes and Diabetic Retinopathy and their Role in Prediction of Progression - an Exploratory Study, BMC Ophthalmol., 2014, vol. 14, no. 1, pp. 89-99.*

3. *M. K. Ikram, C. Y. Cheung, M. Lorenzi, et al., Retinal Vascular Caliber as a Biomarker for Diabetes Microvascular Complications, Diabetes Care, 2013, vol. 36, no. 3, pp. 750–759.*

4. *R. Radha and B. Lakshman, Retinal Image Analysis using Morphological Process and Clustering Technique, Signal Image Process. Int. J., 2013, vol. 4, no. 6, pp. 55–69.*

5. *K. Zorena, D. Raczyńska and K. Raczyńska, Biomarkers in Diabetic Retinopathy and the Therapeutic Implications, Mediators Inflamm., 2013, vol. 2013, Article ID 193604, pp. 1-11.R. E. Sorace, V. S. Reinhardt, and S. A. Vaughn, "High-speed digital-to-RF converter," U.S. Patent 5 668 842, Sept. 16, 1997.*

6. *A. K. McAuley and P. G. Sanfilippo, Vitreous Biomarkers in Diabetic Retinopathy: A Systematic Review and Meta-Analysis, J. Diabetes Complications, 2013, vol. 28, no. 3, pp. 419-425.*

7. *M. D. Abràmoff, M. K. Garvin and M. Sonka, Retinal Imaging and Image Analysis, IEEE Reviews in Biomed. Imaging, 2010, vol. 3, pp. 169–208.*

8. *A. K. Sjølie, R. Klein, M. Porta, et al., Retinal Microaneurysm Count Predicts Progression and Regression of Diabetic Retinopathy. Post-Hoc Results from the DIRECT Programme', Diabetes Med. J. Br. Diabetes Assoc., 2011, vol. 28, no. 3, pp. 345–351.*

9. *R. Vidyasari, I. Sovani, T. L. R. Mengko, et al., Vessel Enhancement Algorithm in Digital Retinal Fundus Microaneurysms Filter for Nonproliferative Diabetic Retinopathy Classification, 2nd ICICI-BME, 2011, Nov. 8-9, pp. 278–281.*

10. *M. Pilch, Y. Wenner, E. Strohmayr, et al., Automated Segmentation of Retinal Blood Vessels in Spectral Domain Optical Coherence Tomography Scans, Biomed. Opt. Express, 2012, vol. 3, no. 7, pp. 1478–1491.*

11. *G. B. Kande, T. S. Savithri and P. V. Subbaiah, Extraction of Exudates and Blood Vessels in Digital Fundus Images, 8th CIT, 2008, July 8-11, pp. 526–531.*

12. *M. K. Ikram, Y. T. Ong, C. Y. Cheung, et al., Retinal Vascular Caliber Measurements: Clinical Significance, Current Knowledge and Future Perspectives, Ophthalmologica, 2013, vol. 229, no. 3, pp. 125–136.*

13. *E. Ezra, E. Keinan, Y. Mandel, et al., Non-Dimensional Analysis of Retinal Microaneurysms: Critical Threshold for Treatment, Integr. Biol. Quant. Biosci. Nano Macro, 2013, vol. 5, no. 3, pp. 474–480.*

14. *R. Ravindraiah and J. L. M. Iqbal, Hard Exudates Detection in Proliferative Diabetic Retinopathy using Gradient Controlled Fuzzy C Means Clustering Algorithm, GESJ Comput. Sci. Telecommun., 2014, vol. 44, no. 4, pp. 27–31.*

15. *Z. Torok, T. Peto, E. Csosz, et al., Combined Methods for Diabetic Retinopathy Screening, Using Retina Photographs and Tear Fluid Proteomics Biomarkers, J. Diabetes Res., 2015, Article ID: 623619, pp 1-8.*

16. *R. Ganjee and B. Gholizadeh, An Improved Retinal Vessel Segmentation Method Based on High Level Features for Pathological Images, J. Med. Syst., 2014, vol. 38, no. 9, pp. 108.*

17. *R. Priya and P. Aruna, Comparison of Gaussian Matched Filter, Kirsch Template and Canny Edge Detection Schemes for Detection of Blood Vessels in Retinal Images, IUP J. Sci. Technol., 2011, vol. 7, no. 4, pp. 31–45.*

18. *G. B. Kande, P. V. Subbaiah, and T. S. Savithri, Unsupervised fuzzy based vessel segmentation in pathological digital fundus images, J. Med. Syst., 2010, vol. 34, no. 5, pp. 849–858.*

19. *S. Deshmukh and S. Patil, Vessel Extraction from Retinal Images by using Matched Filter and First Derivative of Gaussian Function, Int. J. Innov. Res. Electr. Electron. Instrum. Control Eng., 2015, vol. 3, no. 1, 18-22.*

20. *X. Qu, H. Huo, S. Lian, et al., A Novel Frequency Domain Iterative Image Registration Algorithm Based on Local Region Extraction, Math. Probl. Eng., 2015, vol. 2015, Article ID: 215960, pp. 1–8.*

21. *Z. Ghassabi, J. Shanbehzadeh, A. Mohammadzadeh, et al., Colour Retinal Fundus Image Registration by Selecting Stable Extremum Points in the Scale-Invariant Feature Transform Detector, IET Image Process., 2015, vol. 9, no. 10, pp. 889–900.*

22. *Image Sciences Institute: Image Sciences Institute: DRIVE: Digital Retinal Images for Vessel Extraction, [Online], Available: http://www.isi.uu.nl/Research/Databases/DRIVE/. [Accessed: 11-May-2016].*

23. *W.-C. Zhang, F.-P. Wang, L. Zhu, et al., Corner Detection using Gabor Filters, IET Image Process., 2014, vol. 8, no. 11, pp. 639–646.*

24. *F. Farokhian and H. Demirel, Blood Vessels Detection and Segmentation in Retina using Gabor Filters, 10th HONET-CNS, 2013, Dec 11-13, pp. 104–108.*